Published in final edited form as:
J Vasc Interv Radiol. 2008 September ; 19(9): 1347–1353. doi:10.1016/j.jvir.2008.05.007.

Real-Time MRI Guided Laser Atrial Septal Puncture in Swine

Abdalla A. Elagha, MD, **Ozgur Kocaturk, MSc**, **Michael A. Guttman, MSc**, **Cengizhan Ozturk, PhD, MD**, **Ann H. Kim, BSc**, **George W. Burton, BSc**, **June H. Kim, MD**, **Venkatesh K. Raman, MD**, **Amish N. Raval, MD**, **Victor J. Wright, BSc**, **William H. Schenke, BA**, **Elliot R. McVeigh, PhD**, and **Robert J. Lederman, MD**

From (1) the Division of Intramural Research (AAE, OK, MAG, CO, AK, JHK, VKR, ANR, VJW, WHS, ERM, RJL), National Heart Lung and Blood Institute, National Institutes of Health, Bethesda, MD, USA, and (2) Spectranetics (GWB), Colorado Springs, CO, USA

Abstract

Purpose—Even in experienced hands, X-ray guided needle atrial septal puncture risks non-target perforation and pericardial tamponade. Real-time MRI offers potentially superior target imaging and multiplanar device tracking. We report initial preclinical experience with real-time MRI-guided atrial septal puncture using a MRI-conspicuous blunt laser catheter that perforates only when energized.

Materials and Methods—We customized a clinical excimer laser catheter (0.9mm Clirpath, Spectranetics) with a receiver coil to impart MRI visibility at 1.5T. Seven swine underwent laser transseptal puncture under real-time MRI. MRI signal-to-noise profiles were obtained of the device *in vitro*. Tissue traversal force was tested with a calibrated meter. Position was corroborated by pressure, oximetry, angiography, and necropsy. Intentional non-target perforation simulated serious complication.

Results—Embedded MRI-antennae accurately reflected the position of the laser catheter tip and profile *in vitro* and *in vivo*. Despite increased profile from the microcoil, the 0.9mm laser catheter traversed *in vitro* targets with similar force (0.22 ± 0.03N) compared with the unmodified laser.

Laser puncture of the atrial septum was successful and accurate in all animals. The laser was activated an average 3.8 ± 0.4 seconds before traversal. There were no sequelae after 6 hour observation. Necropsy revealed 0.9mm holes in the fossa ovalis in all animals.

Intentional perforation of the aorta and of the atrial free wall was evident immediately.

Conclusion—MRI-guided laser puncture of the interatrial septum is feasible in swine, and offers controlled delivery of perforation energy using an otherwise blunt catheter. Instantaneous soft-tissue imaging provides immediate safety feedback.

Introduction

Transcatheter needle puncture of the interatrial septum is a critical component of several diagnostic and therapeutic cardiovascular procedures. Conventional needle puncture is guided by tactile and fluoroscopic visual feedback during catheter manipulation, rather than by

Address for Correspondence: Robert J. Lederman, MD, Translational Medicine Branch, Division of Intramural Research, National Heart Lung, and Blood Institute, National Institutes of Health, Building 10, Room 2c713, MSC1538, Bethesda, MD 20892-1538, USA. Telephone: +1-301-402-6769. Email: ledermar@nhlbi.nih.gov.
AAE and OK contributed equally to this project.

Conflicts of Interest

Spectranetics customized laser catheters under a Collaborative Research and Development Agreement with NHLBI. George Burton is an employee of Spectranetics.

No other authors have a conflict of interest.

imaging of the target tissue (1–6). This may account even in contemporary series for occasional inadvertent puncture of the aortic root(7,8), or puncture at a location unfavorable for the catheter procedure(9–11). In addition, the puncture needle accumulates force that is released abruptly during crossing. This can lead to inadvertent puncture of non-target tissue such as the left atrial free wall. Puncture using a small laser catheter instead of a needle has the advantage of a blunt instrument that perforates tissue only during controlled activation, and that requires ten-fold less force than a needle(12).

Real-time MRI is being developed to guide catheter-based treatments that exploit the unique tissue imaging capabilities, arbitrary views, and freedom from ionizing radiation afforded by MRI (reviewed in (13)). We(14) and others(15) have demonstrated successful image-guided needle septal puncture using real-time MRI in swine. Here we describe a laser catheter that is conspicuous under MRI and test its utility *in vivo*. We hypothesize that laser septal puncture can be conducted effectively and safely using MRI as a single imaging modality. Related image-guided laser procedures may have value in the future, creating complex non-anatomic vascular connections, such as transcatheter intrahepatic shunts and extraanatomic bypass.

Materials and Methods

Animal Protocol

Nonsurvival animal procedures were approved by the National Heart Lung and Blood Institute Animal Care and Use Committee. Naïve Yorkshire swine (mean 66± 9 kg) underwent anesthesia induced with tiletamine, zolazepam, and xylazine and maintained with inhaled isoflurane 2%. Femoral veins were accessed percutaneously. At the conclusion of experiments, animals were euthanized with potassium chloride 4 mEq/kg. Necropsy specimens were inspected for target lesion success and for evidence of thermal injury.

Interventional Magnetic Resonance Imaging

Procedures were conducted in a combined X-ray (Axiom Artis FC, Siemens, Erlangen, Germany) and 1.5T MRI (Sonata or Espree, Siemens) interventional suite, customized for real-time MRI(16). During acquisition, MRI data were transferred to an external workstation for real-time reconstruction and customized 2D/3D image display. Hemodynamics, scan control, and image data were displayed inside the scanner room using shielded LCD projectors. Instantaneous hemodynamic monitoring included oximetry, two-channel invasive blood pressure, and surface electrocardiogram (Magnitude CV, In-Vivo Research, Orlando, FL). Standard 6 or 8 channel phased array torso and spine surface coils were used (Siemens). The operators and staff communicated via directional optical microphones (Phone-Or, Or-Yehuda, Israel) and RF-filtered headsets for audio noise suppression (Magnacoustics, Atlantic Beach, NY).

Interactive, multi-slice real-time MRI used steady state free precession (SSFP) pulse sequences. Typical parameters were: repetition time (TR) 3 ms, echo time (TE) 1.5 ms, flip angle 45°, bandwidth 800 Hz/pixel, field of view (FOV) 32 × 24 cm, matrix 192 ×108, generating 1.7 × 2.2 × 6 mm voxels. Using 3/4; partial phase k-space coverage and echo-sharing, an imaging rate of 8 frames/sec was achieved with an acquisition-to-display latency of approximately 250 ms. Images reconstructed from active device signals were color highlighted and blended with surface coil images to highlight catheter position in relation to soft tissue anatomy (17) When required, catheters could be visualized even when outside of selected scanning slabs by selecting (X-ray-like device-only) projection mode MRI, which displays only the active catheters in a very thick slice. Saturation pre-pulses were toggled on/off during real-time imaging to suppress background tissue when gadolinium contrast enhancement was desired. Multiple oblique slices were acquired in rapid succession,

repositioned interactively, or individually omitted and reapplied as desired. The slices were rendered in 3D to show their relationship to each other.

Catheter Devices

"Active" MRI Laser Catheters—Clinical ultraviolet (308nm) fiberoptic laser ablation catheters (Clirpath X-80, Spectranetics, Colorado Springs, CO) were modified with receiver coils (antennae) to make them conspicuous under MRI (Figure 1). The loop antenna design included a distal microcoil to create a bright spot near the laser catheter tip. The catheter connected via micro coaxial cable to tuned matching and decoupling circuitry(14,18), designed to attenuate heating during MRI radiofrequency excitation, and was connected to a separate MRI receiver channel. The radiofrequency coil increased the laser catheter outer diameter from 0.9mm to 1.5mm. The catheter retained a 0.0155″ inner lumen suitable for delivery of a 0.014″ guidewire or for transducing pressure. Compared with a Brockenbrough needle, the off-the-shelf laser significantly attenuated pressure waveforms but was still adequate to distinguish right and left heart atrial recordings (12). The fiberoptic transmission line was extended 8m to connect through a waveguide (portal through the RF shield) to the laser console positioned outside the radiofrequency shielded MRI room. The energy source was an unmodified clinical CVX-300 Excimer Laser System (Spectranetics) set to deliver 25 laser pulses per second at a fluence of 45 mJ/mm^2).

Catheter MRI signal profiles were obtained in a saline phantom, normalized for noise, and depicted as signal-to-noise ratio images(19) using Matlab v7.0.4 (The MathWorks, Inc., Natick, MA) and Medical Image Processing Analysis and Visualization software (http://mipav.cit.nih.gov/, Bethesda, Maryland).

"Active" MRI guidewire—A 0.035″ active dipole guidewire, with a flexible tip, was constructed to deliver introducer sheaths into the atria. The dipole design rendered the wire conspicuous along its profile, and decoupling circuitry limited heating during MRI.

"Passive" MRI catheter devices—Commercial 9Fr Mullins introducer sheaths (Cook, Bloomington, IN) were modified with a 1mm segment of 0.0009″ 304V medical grade stainless steel guidewire glued to the distal tip to create a susceptibility artifact ("black spot") during MRI.

Force measurements—The force required to effect perforation(12) was tested *in vitro* comparing a modified active laser catheter and an unmodified 0.9mm laser catheter. A digital force meter (Model ZPH, Imada Inc., Northrbook, IL) was attached near the tip of the test catheter and sampled at 1000 Hz. The activated laser (45 mJ/mm^2 at 25 pulses/s) was advanced using the force meter across freshly explanted porcine interatrial septal tissue outside the fossa ovalis.

Imaging Phantom Experiments—We tested the MRI receiver coil performance of the active laser device using an in vitro phantom. A custom acrylic platform incorporating calibrated fluid wells served to stabilize the laser catheter and provide reference position markers during SSFP MRI. The test device was connected via Siemens Flex coil adaptor to the scanner receiver chain, and placed within the head transmit coil.

Transseptal Laser Catheterization

Baseline MRI verified there was no pre-existing patent foramen ovale or atrial septal defect. Passive introducer sheaths were delivered into the right atrium under real-time MRI over the active guidewire. Using multiple orthogonal views of the atrial septum, the delivery system was manipulated under real-time MRI using a blunt mandril to appose the fossa ovalis. ECG-

gated MRI verified sheath position before the mandril was removed and the laser catheter introduced to the sheath tip.

The position of the active laser catheter was confirmed and then laser energy was delivered with continuous MRI guidance until the laser catheter entered the left atrium.

Atrial position was confirmed by imaging, by pressure waveforms transduced through the guidewire lumen, by hemoglobin oximetry of aspirated left atrial blood, and by injections of dilute gadopentate dimeglumine 10% (Magnevist, Bayer Healthcare, Leverkusen, Germany). Finally the introducer sheath could be advanced using the laser catheter as a rail across the atrial septum into the left atrium.

In one additional (eighth) animal, the aorta and the left atrial free wall deliberately were perforated to test the utility of the imaging system to detect serious complications.

Statistics

Continuous parameters were reported as mean ± standard deviation, and compared using two-tailed paired t tests.

Results

In vitro tests

The microcoil embedded at the tip of the laser catheter (Figure 1) made the device conspicuous by creating characteristic bi-lobed bright spots on MR images (Figure 2).

The modified MRI-active laser catheter was thicker than the unmodified catheter (1.5 vs 0.9mm). This did not increase the force required to cross freshly explanted extra-fossal atrial septal tissue (active 0.22 ± 0.03 N versus unmodified 0.21 ± 0.07 N, Figure 3). By comparison this was approximately ten times less than the force required to cross using a conventional Brockenbrough needle (12).

In vivo tests

MRI and catheter probing confirmed no patent foramen ovale in all animals. MRI-guided laser atrial septal puncture was successful in all seven animals. A representative real-time MRI puncture sequence is shown in Figure 4. In this initial experience, puncture required 31 ± 9 minutes from the initiation of real-time MRI for positioning of passive catheter devices. Laser energy was applied for an average of 3.8 ± 0.4 seconds before crossing. One procedure was prolonged because a damaged device was only intermittently conspicuous. Laser activation did not create imaging artifacts or otherwise disrupt imaging.

We interactively applied device-only projection mode to confirm the location of the laser catheter tip in case it has exited the imaging slice (Figure 5). The supplementary video demonstrates safe atrial septal puncture using this technique even very close to the aorta.

Minimal force is applied to the laser catheter during energy delivery. Advancing the laser catheter did not, for example, “back out” or displace the coaxial introducer sheath during septal crossing. Left atrial entry was confirmed by pressure waveforms (right atrial mean 5±0.6, left atrial pressure 9 ± 1.1 mmHg), hemoglobin oximetry (right atrial 76±3.1%, left atrial 96±0.8%). Injection of gadopentate dimeglumine 10% into the left atrium, which has a known nonlinear T1-concentration relationship, opacifies all left-sided blood and is comparably more sensitive for left atrial position than dilute radiocontrast injections into the left atrium (data not shown).

After atrial septal puncture, animals were observed for 5.8 ± 1.1 hours without pericardial effusion or other complications.

After intentional perforation of the aorta, a jet of dephased blood immediately was evident on real-time SSFP MRI (Figure 6). This was not apparent during hemodynamic monitoring. After intentional perforation of the left atrial free wall and of the left atrial appendage, accumulation of blood in the pericardium was immediately evident on real-time SSFP MRI. Similarly there were no hemodynamic changes during a two hour observation period.

After successful transseptal puncture, necropsy examination of the endocardium revealed no thermal or mechanical injury. The puncture was found in the fossa ovalis in all animals. The laser puncture hole had smooth contours but demonstrated elastic recoil. With tension sufficient to “flatten” the tissue, the laser-created hole was 0.9mm, compared with fiberoptic laser bundle diameter of 0.9mm and the MRI-modified device having an outer diameter of 1.5mm.

Discussion

We have demonstrated catheter-based laser puncture of the interatrial septum guided entirely by real-time MRI in normal swine. The blunt-tipped laser catheter was manipulated safely within cardiac chambers and created injury only when ablation energy was applied by the operator at the desired time and place. Modifications rendered the clinical laser catheter conspicuous under MRI. Real-time MRI assured accurate positioning before laser ablation and septal traversal.

Real-time MRI is under development to guide catheter-based procedures that take advantage of soft-tissue, blood space, and other contrast mechanisms. In animals, demonstrations include arterial angioplasty and stenting(20), myocardial cell and gene delivery(21), transcatheter cardiac valve deployment(22), and endograft deployment(23). Human diagnostic cardiovascular catheterization(24,25), peripheral artery angioplasty(26), and coarctation angioplasty(27) also have been reported. Future applications of real-time MRI will include catheter-based extra-anatomic bypass, which require flexible devices —such as the MRI laser used here — to traverse tissue boundaries in controlled fashion.

Conventional catheter devices generally are unsuitable for operation under MRI. Most have steel braiding that produce large image artifacts and risk heating by induced currents, yet remain inconspicuous because they lack water protons. We favor incorporating antennae into catheter devices. Such “active” catheter devices appear conspicuous because they detect nearby excited proton spins. They are connected to separate MRI scanner receiver channels, allowing catheter-related signals to be displayed in color to improve visibility

For this experiment, fiberoptic laser catheters were modified to incorporate receiver coils that permitted visualization both of a microcoil at the tip and of a dipole antenna along the catheter shaft. The fiberoptic transmission line was extended so that the laser console, which generates radiofrequency noise that interferes with MRI, could be positioned outside the shielded MRI room. While the receiver coils significantly increased the outer diameter of the laser catheters in this proof-of-principle experiment, catheters retained the ability to traverse the atrial septum with minimal displacement force. In our tests, laser septal traversal requires ten-fold less forward force than does conventional needle septal puncture (12). Further miniaturization is feasible.

Transvenous atrial septal puncture permits access to the left atrium for balloon mitral valvuloplasty, for radiofrequency ablation of arrhythmia including atrial fibrillation, and for investigational left atrial appendage occlusion and mitral valve repair.

Even in experienced hands, conventional x-ray guided transseptal puncture confers a discrete risk of serious complications including pericardial tamponade and aortocameral fistula. These are more common in patients with abnormal atrial septal geometry, in whom tactile landmarks from the vena cava, aorta, and limbus fossa ovalis less reliably predict the location of the fossa ovalis, and in patients with small left atria, in whom forward puncture force may drive the needle across both septum and left atrial free wall (28). Ultrasound guidance has become popular (29) but fails to identify the needle tip when outside the selected imaging plane (11). This may increase the risk of unintentional or inaccurate puncture. By contrast, the device tip can always be discovered in real-time MRI with interactive “device-only projection mode”. An alternative approach to the same problem might include automated tracking microcoils on the catheter tip using special magnetic resonance pulse sequences, which also can be used automatically to adjust other MRI parameters including slice location(30). Multiplanar real-time MRI allows simultaneous visualization of the device, the fossa ovalis and other landmarks, and likely will guide catheter manipulation even when the septal contour is distorted, thickened, or contain prosthetic material. Real-time MRI also can provide immediate evidence of serious complications resulting from unintentional perforation(31).

Like a Brockenbrough transseptal needle, the laser catheter retains a central lumen that can be used to transduce pressures (albeit overdamped), inject contrast, or deliver a guidewire. Because it is blunt, the laser catheter can be used safely as a rigid rail to deliver sheaths or other catheter devices to any left atrial location without further device exchange.

During transluminal angioplasty, displacement of blood and contrast by continuous saline flush reduces cavitation injury of the vessel wall (32). In our experience, septal ablation lesions were sharply demarcated without saline infusion.

These experiments were conducted in healthy swine which may not model the challenges of atrial septal puncture in humans with distorted, scarred, or patched septal anatomy. To guide the active laser catheter, we used MRI-passive soft Mullins-type sheaths that are inconspicuous under MRI and that are designed for use in tandem with rigid Brockenbrough needles. More sophisticated MRI-active deflectable introducer sheaths would simplify the conduct of MRI laser septal puncture. Because they are thin-walled, the atrial septum and fossa ovalis can not be identified *en face* under segmented or real-time MRI; however, attainable MRI views resemble conventional bi-atrial views employed under ultrasound. For these nonclinical experiments, we did not conduct formal heating testing of the active MRI catheters, since the decoupling techniques have been described elsewhere (33). Contemporary reports from experienced operators suggest a relatively low complication rate (<1%) using X-ray fluoroscopy with electrophysiology catheters for landmarks (8,34) and using a guidewire to avoid inadvertent left atrial free wall puncture (34,35), although risks may be higher in more complex anatomy or with less-experienced operators. Other advanced manipulation and guidance systems are under development, including robotic systems (36).

Active MRI laser catheters, which can traverse tissue boundaries under direct image guidance in any arbitrary plane or orientation, may have utility in a range of novel catheter-based interventional procedures such as extra-anatomic bypass.

Transvenous laser septal puncture can be conducted accurately and safely, entirely under real-time MRI guidance in swine. The blunt-tip laser catheter does not risk perforation except when activated, and crosses target tissues with minimal force that may be less likely to “jump” across the left atrial free wall. Unlike intracardiac or transesophageal echocardiography, where the location of the catheter tip can be misidentified when it is out-of-plane, the tip of this active MRI laser catheter can be kept in view, as can the soft-tissue target. Intentional perforation of the atrial free wall or aorta is evident immediately because of the large field of view readily

available during MRI, suggesting a potential safety benefit of combined MRI catheter and tissue imaging.

Supplementary Material

Refer to Web version on PubMed Central for supplementary material.

Acknowledgements

The authors thank Kathy Lucas and Joni Taylor for their animal care and support, and Parag V. Karmarkar for assistance with decoupling circuitry. Spectranetics customized laser catheters under a Collaborative Research and Development Agreement with NHLBI. Supported by the NHLBI Division of Intramural Research (Z01-HL005062-04 CVB).

References

1. Brockenbrough EC, Braunwald E, Ross J Jr. Transseptal left heart catheterization. A review of 450 studies and description of an improved technic. Circulation 1962;25:15–21. [PubMed: 13873261]
2. Mullins CE. Transseptal left heart catheterization: experience with a new technique in 520 pediatric and adult patients. Pediatr Cardiol 1983;4:239–45. [PubMed: 6647111]
3. Clugston R, Lau FY, Ruiz C. Transseptal catheterization update 1992. Cathet Cardiovasc Diagn 1992;26:266–74. [PubMed: 1394413]
4. Roelke M, Smith AJ, Palacios IF. The technique and safety of transseptal left heart catheterization: the Massachusetts General Hospital experience with 1,279 procedures. Cathet Cardiovasc Diagn 1994;32:332–9. [PubMed: 7987913]
5. Croft CH, Lipscomb K. Modified technique of transseptal left heart catheterization. J Am Coll Cardiol 1985;5:904–10. [PubMed: 3973292]
6. El-Said HG, Ing FF, Grifka RG, et al. 18-year experience with transseptal procedures through baffles, conduits, and other intra-atrial patches. Catheter Cardiovasc Interv 2000;50:434–9. [PubMed: 10931616]
7. Liu TJ, Lai HC, Lee WL, et al. Immediate and late outcomes of patients undergoing transseptal left-sided heart catheterization for symptomatic valvular and arrhythmic diseases. Am Heart J 2006;151:235–41. [PubMed: 16368324]
8. De Ponti R, Cappato R, Curnis A, et al. Trans-septal catheterization in the electrophysiology laboratory: data from a multicenter survey spanning 12 years. J Am Coll Cardiol 2006;47:1037–42. [PubMed: 16516090]
9. Hung JS. Atrial septal puncture technique in percutaneous transvenous mitral commissurotomy: mitral valvuloplasty using the Inoue balloon catheter technique. Cathet Cardiovasc Diagn 1992;26:275–84. [PubMed: 1394414]
10. Linker NJ, Fitzpatrick AP. The transseptal approach for ablation of cardiac arrhythmias: experience of 104 procedures. Heart 1998;79:379–82. [PubMed: 9616347]
11. Bazaz R, Schwartzman D. Site-selective atrial septal puncture. J Cardiovasc Electrophysiol 2003;14:196–9. [PubMed: 12693505]
12. Elagha AA, Kim AH, Kocaturk O, Lederman RJ. Blunt atrial transseptal puncture using excimer laser in swine. Catheter Cardiovasc Interv 2007;70:585–90. [PubMed: 17896413]
13. Lederman RJ. Cardiovascular interventional magnetic resonance imaging. Circulation 2005;112:3009–17. [PubMed: 16275886]
14. Raval AN, Karmarkar PV, Guttman MA, et al. Real-time MRI guided atrial septal puncture and balloon septostomy in swine. Catheter Cardiovasc Interv 2006;67:637–43. [PubMed: 16532499]
15. Arepally A, Karmarkar PV, Weiss C, Rodriguez ER, Lederman RJ, Atalar E. Magnetic resonance image-guided trans-septal puncture in a swine heart. J Magn Reson Imaging 2005;21:463–7. [PubMed: 15779027]
16. Guttman MA, Ozturk C, Raval AN, et al. Interventional cardiovascular procedures guided by real-time MR imaging: an interactive interface using multiple slices, adaptive projection modes and live 3D renderings. J Magn Reson Imaging 2007;26:1429–35. [PubMed: 17968897]

17. Aksit P, Derbyshire JA, Serfaty JM, Atalar E. Multiple field of view MR fluoroscopy. Magn Reson Med 2002;47:53–60. [PubMed: 11754442]
18. Susil RC, Yeung CJ, Atalar E. Intravascular extended sensitivity (IVES) MRI antennas. Magn Reson Med 2003;50:383–90. [PubMed: 12876715]
19. Constantinides CD, Atalar E, McVeigh ER. Signal-to-noise measurements in magnitude images from NMR phased arrays. Magn Reson Med 1997;38:852–7. [PubMed: 9358462]
20. Buecker A, Neuerburg JM, Adam GB, et al. Real-time MR fluoroscopy for MR-guided iliac artery stent placement. J Magn Reson Imaging 2000;12:616–22. [PubMed: 11042645]
21. Dick AJ, Guttman MA, Raman VK, et al. Magnetic resonance fluoroscopy allows targeted delivery of mesenchymal stem cells to infarct borders in Swine. Circulation 2003;108:2899–904. [PubMed: 14656911]
22. Kuehne T, Yilmaz S, Meinus C, et al. Magnetic resonance imaging-guided transcatheter implantation of a prosthetic valve in aortic valve position: Feasibility study in swine. J Am Coll Cardiol 2004;44:2247–9. [PubMed: 15582324]
23. Raman VK, Karmarkar PV, Guttman MA, et al. Real-time magnetic resonance-guided endovascular repair of experimental abdominal aortic aneurysm in swine. J Am Coll Cardiol 2005;45:2069–77. [PubMed: 15963411]
24. Razavi R, Hill DL, Keevil SF, et al. Cardiac catheterisation guided by MRI in children and adults with congenital heart disease. Lancet 2003;362:1877–82. [PubMed: 14667742]
25. Kuehne T, Yilmaz S, Schulze-Neick I, et al. Magnetic resonance imaging guided catheterisation for assessment of pulmonary vascular resistance: in vivo validation and clinical application in patients with pulmonary hypertension. Heart 2005;91:1064–9. [PubMed: 16020598]
26. Paetzel C, Zorger N, Bachthaler M, et al. Magnetic resonance-guided percutaneous angioplasty of femoral and popliteal artery stenoses using real-time imaging and intra-arterial contrast-enhanced magnetic resonance angiography. Invest Radiol 2005;40:257–62. [PubMed: 15829822]
27. Krueger JJ, Ewert P, Yilmaz S, et al. Magnetic resonance imaging-guided balloon angioplasty of coarctation of the aorta: a pilot study. Circulation 2006;113:1093–100. [PubMed: 16490822]
28. Mullins, CE. Transseptal left heart catheterization. In: Mullins, CE., editor. Cardiac catheterization in congenital heart disease: pediatric and adult. Malden, MA: Blackwell Publishing; 2006. p. 223-54.
29. Ren, JF.; Callans, D.; Marchlinski, FE.; Schwartzman, D. Practical intracardiac echocardiography in electrophysiology. Malden, MA: Blackwell Publishing; 2005.
30. Elgort DR, Wong EY, Hillenbrand CM, Wacker FK, Lewin JS, Duerk JL. Real-time catheter tracking and adaptive imaging. J Magn Reson Imaging 2003;18:621–6. [PubMed: 14579407]
31. Raval AN, Telep JD, Guttman MA, et al. Real-time magnetic resonance imaging-guided stenting of aortic coarctation with commercially available catheter devices in Swine. Circulation 2005;112:699–706. [PubMed: 16043639]
32. Tcheng JE. Saline infusion in excimer laser coronary angioplasty. Semin Interv Cardiol 1996;1:135–41. [PubMed: 9552504]
33. Ocali O, Atalar E. Intravascular magnetic resonance imaging using a loopless catheter antenna. Magn Reson Med 1997;37:112–8. [PubMed: 8978639]
34. Cheng A, Calkins H. A conservative approach to performing transseptal punctures without the use of intracardiac echocardiography: stepwise approach with real-time video clips. J Cardiovasc Electrophysiol. 2007
35. Hildick-Smith D, McCready J, de Giovanni J. Transseptal puncture: use of an angioplasty guidewire for enhanced safety. Catheter Cardiovasc Interv 2007;69:519–21. [PubMed: 17286295]
36. Saliba W, Cummings JE, Oh S, et al. Novel robotic catheter remote control system: feasibility and safety of transseptal puncture and endocardial catheter navigation. J Cardiovasc Electrophysiol 2006;17:1102–5. [PubMed: 16879628]

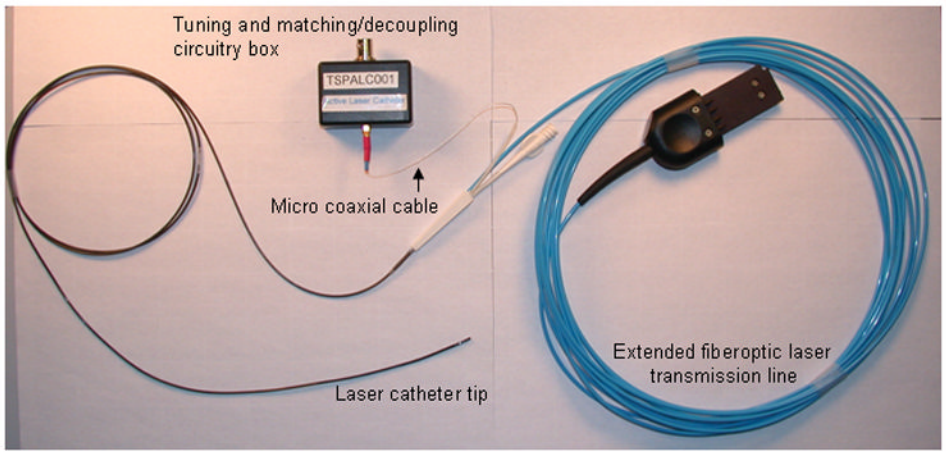

Figure 1.
The commercial 0.9mm excimer laser catheter is modified with a microcoil at the distal tip connected via a microcoaxial cable that serves as a dipole antenna. The fiberoptic shaft is lengthened 8 meters in order to connect to a laser console positioned outside the shielded MRI lab. The resulting “active” catheter antenna connects to the MRI system to impart visibility during imaging.

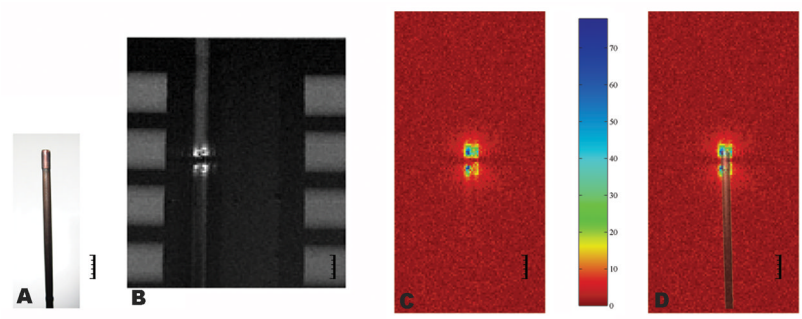

Figure 2.

Signal-to-noise (SNR) profile of the active laser catheter. The calibration mark = 5mm. (A) An insulated copper microcoil is evident at the tip of the modified laser catheter. (B) MRI of the active laser catheter in a calibrated geometry phantom. (C) The signal profile is mapped in normalized SNR units, and also displayed with a photographic overlay of the catheter in (D). The signal profile is larger than the catheter tip.

Figure 3.
Representative force-versus-time curves of unmodified (passive, continuous) and modified (active, dotted line) laser catheters crossing porcine interatrial septal tissue *ex vivo*. Force declines precipitously when the laser crosses tissue (arrows). Both catheters accumulated comparable force before perforation.

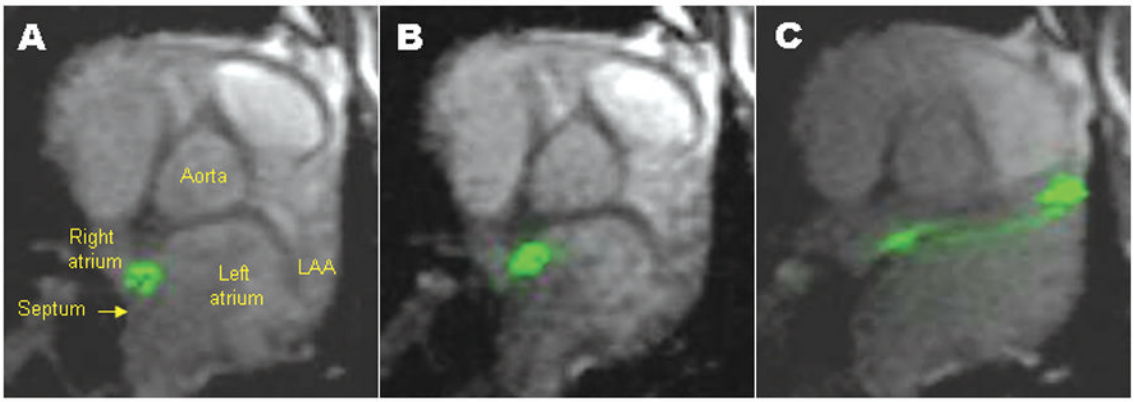

Figure 4.
A representative MRI laser septal puncture procedure. (A) The tip of the active laser is engaged against the fossa ovalis and causes characteristic “tenting” appearance. (B) The activated laser crosses into the left atrium. (C) The blunt catheter is advanced into the left atrial appendage (LAA).

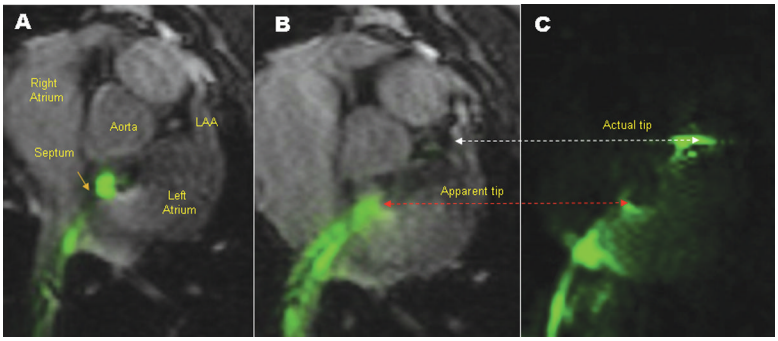

Figure 5.
Projection mode unambiguously displays catheter tips that are outside selected imaging slices. (A) shows anatomic references during real-time SSFP MRI. (B) Tomographic image of a laser catheter in the left atrium, which appears to be located near the interatrial septum (dotted red double-arrow). (C) Projection-mode image demonstrates that the tip of the catheter is instead near the lateral wall of the left atrium (dotted white double-arrow indicates corresponding points on the two images).

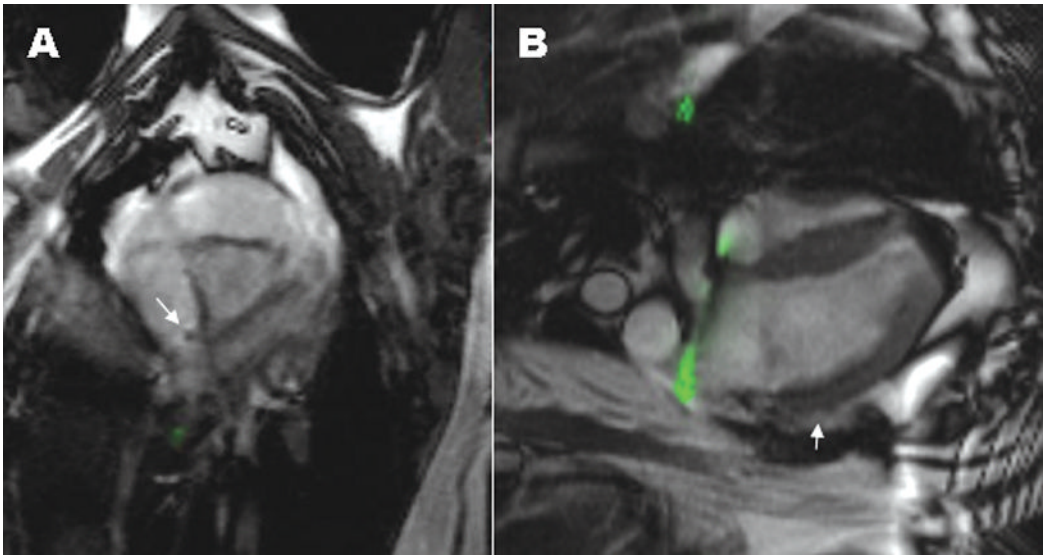

Figure 6.
Intentional perforation under real-time SSFP MRI. (A) The aortic root is perforated and a jet of dephased spins appears black within the right atrium (arrow). (B) The left atrial appendage is perforated and a small effusion accumulates within the pericardium (arrow). Both findings were subtle on MRI and not detectable hemodynamically